Effects in Extreme Ultraviolet and in Magnetic Field Observed during Stealth CME Formation, Geomagnetic Responses to Its Impact on the Magnetosphere

Iu.S. Zagainova [1], V.G. Fainshtein [2], L.I. Gromova [1], S.V. Gromov [1]

[1] Pushkov Institute of Terrestrial Magnetism, Ionosphere and Radio Wave Propagation RAS, Moscow, Russia

[2] Institute of Solar-Terrestrial Physics SB RAS, Irkutsk, Russia

E mail (mailto:yuliazagainova@mail.ru).

Accepted: 28 May 2019

Abstract By example of the 16 June 2010 event, stealth coronal mass ejection (Stealth-CME) emergence is shown to be probably accompanying by various manifestations of small-scale activity in the solar atmosphere and some features of variations in the magnetic field parameters. We also discuss the response of the geomagnetic field to the effect of this CME on the Earth magnetosphere.

Keywords: Sun, coronal mass ejection, solar wind-magnetosphere interaction, interplanetary magnetic field.

1 - INTRODUCTION

The vast majority of the coronal mass ejections (CMEs) recorded in coronagraph field-of-view (FOV) is associated with various manifestations of the solar activity in emission corona (low coronal signatures - LCSs): flares, filament eruptions, EUV waves, dimming, jets, etc. Contrary to this, there are such CMEs, observed by coronagraphs, those are not associated with LCSs. At present, CMEs without LCSs are called stealth CMEs (D'Huys et al., 2014). For a long time, it was considered that such CMEs were launched from the backside of the Sun relative to the observer. Robbrecht, et al. (2009) first showed that a stealth CME could be observed in the visible part (3) of the Sun and Ma et al. (2010) compared the properties of CMEs with and without LCSs. Howard T.A., et al (2013) supposed that the absence of LCSs in a CME initiation process could be most likely caused by low time and spatial resolution, and low sensor sensitivity of recording equipment at the telescopes. In other words, they believe that stealth CMEs out be also followed by different effects of the solar activity, such as flares, filament eruptions and others, but they could not be registered by the equipment.

It is accepted today that filament eruption is a trigger for the most CMEs (Schmieder et al., 2013). The authors note that more than 80% of eruptions lead to a CME. As highlighted, no filament eruption precedes a stealth-CME. Thus, we could expect the mechanism of a stealth-CME generation differs from the generation mechanism of the most non-stealth-CME, but details of this mechanism remain unknown.

D'Huys et al. (2014) studied 40 events of stealth-CMEs observed at 2012. Their total list of stealth-CMEs is the longest to date one. The authors have suggested a definition of stealth-CMEs as coronal mass ejections that are initiated in the visible part of the Sun but are not followed by LCSs. It was shown that an average speed of the listed stealth-CMEs is equal about 300 km/s. It is more less than an average linear speed of CMEs with LCSs of 435 km/s. The angular widths of stealth-CMEs turned out more narrow (~25^0) than the angular widths of CMEs with LCSs (~ 35^0).

And, finally, though the principal angle (PA) of stealth-CMEs can take any values within the [0^o – 360^o] range, but it's far more likely that PA of stealth-CMEs is equal 0^0 (or 360^0 which is the same). It should be noted that using PA of stealth-CMEs observed simultaneously in LASCO coronagraphs FOV and STEREO (A or B COR2 coronagraphs), D'Huys et al. (2014) suggested the method to determine a initiation source location of stealth CMEs on the Sun disk (the front or backside of the Sun relative to the observer), where stealth-CMEs launched from.

Using improved pre-processing data methods for analyzing of solar images observed with high temporal and spatial resolution SDO space telescopes in different spectral channels, Alzate et al. (2017) identified a LCSs followed by formation stage of each stealth-CMEs.

The authors considered the same stealth-CMEs as in D'Huys et al. (2014). They have also concluded that all 40 stealth CMEs were associated with some form of LCSs (small flares, jets, or filament eruptions), and on the whole, the very fact, that the listed mass ejections were identified as stealth-CMEs, was caused by limitations of space-time resolution of the telescope and pre-processing data methods.

Despite these positive experiences, the challenge remains to detect of stealth-CME initiation sources on the solar disk. Hence, development of new methods to detect the source location and time moment of stealth-CME initiation is an acute problem.

We suppose that any solar activity should be always followed by stealth-CME initiation stage and especially after impulse start of the mass ejection moving, due to sharp increasing of translational motion of the leading edge of its frontal structure is one of the main causes of the plasma perturbation and the magnetic field variations. This fact may be a proxy of detection of a stealth-CME initiation source.

As a rule, the formation of the most part of CME frontal structure (FS) is associated with the solar activity in the lower emission corona. It is possible to observe manifestations of the solar activity within the area on the solar disk, which is described by relatively great spatial sizes (about tens or hundreds arcsecs) for a long time (from several tens of minutes up to several hours). Besides, visual analysis of CME formation basing on the solar EUV images allows us to conclude that stealth-CMEs could also be followed by different manifestations of the short-time small-scale solar activity. For example, in one of the first studies [Gallagher et al., 2003)] authors shown that formation of a CME as large-scale structure was preceded by a short-term EUV brightening in several small-scale magnetic structures of the lower solar corona. We hypothesized that such short-time small-scale solar activity could also be associated with stealth-CME formation.

Usually formation of CMEs with LCSs is also followed by reorganization of magnetic field configuration in the solar photosphere. Such magnetic field restructuring is often associated with emersion of a new magnetic flux (Feynman and Martin, 1995), active magnetic field canceling (Sterling et al., 2010) and others. It follows that formation and moving of stealth-CMEs

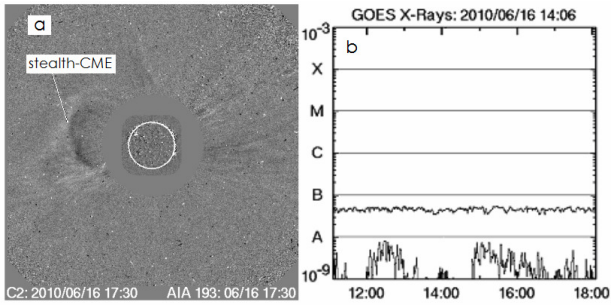

Fig. 1. a) – The stealth-CME observed in LASCO C2 FOV on 2010 June 16; b) –GOES SXR flux. Upper curve is SXR flux in the wavelength range of 1 – 8 Å, lower curve is the same as upper curve but in the wavelength range of 0.5 – 4 Å.

could lead to variations of photosphere magnetic field as well. As far as we know, to date this problem has not been discussed in literature and one of aims of our study is to fill this gaps.

Some researchers studied the formation stage of LCSs-associated CMEs using data with high temporal and spatial resolution from SDO/AIA telescopes (for example, see Fainshtein and Egorov, 2015; Zagainova and Fainshtein, 2015; Grechnev et al., 2016). The authors detected frontal structures (FS) of many CMEs in the lower solar corona and investigated FS kinematics in SDO FOV. But it is unknown whether it is possible to detect formation of a stealth-CME FS. The second aim of this paper is to describe our approach to solving this problem.

It was established (Heber B., et al., 2015) when stealth-CMEs approach the Earth they could cause Forbush decreases. Some researchers (for example, see Nieves-Chinchilla et al., 2013; Kilpua et al., 2014; Nitta and Mulligan, 2017) suppose that the geomagnetic field disturbances could be caused by a stealth-CME effect on the Earth magnetosphere. He et al. (2018) showed that even a weak and low CME without LCSs detected on 8 October 2016 caused a relatively intense geomagnetic storm.

The aim of this paper is the presentation of a new approach to detect source location and initiation time of a stealth-CME on the solar disk and case study of the stealth-CME observed in LASCO C2 FOV on 2010 June 16 at 14:54:05 UT. The response of the magnetosphere and the magnetic field of the Earth to this stealth-CME are discussed as well.

2 - Materials and methods

We studied the solar activity accompanying the initiation of the stealth-CME recorded with the LASCO C2 FOV onboard SOHO, on 16 June 2010 (14:54:05 UT) (Fig. 1a). This CME was identified by Heber et al. (2014) as a stealth-CME.

Our analyze showed that this CME can be identified a stealth-CME due to an absence of a X-ray or optical-intensity flares, which often accompany a non-stealth-CME initiation phase (see Fig. 1b), an absence of a filament eruption, which could be observed on 304 Å or H_α images, and an absence of coronal dimmings which are often been visible on the solar disk after a CME launch as well. This CME has been initiated in the visible part of the Sun so as evidenced by the interplanetary CME (ICME) reached the Earth on 2010 June 21 according to the CME velocity registered by LASCO C3 FOV. In the catalog from https://cdaw.gsfc.nasa.gov/CME_list/ one can see some the CME characteristics such as central position angle PA = 61°, angular width AW = 153° (partial halo CME), linear projection velocity V_{lin} = 236 km/s, acceleration a = 6.5 m/s^2, mass m = $6.8 \cdot 10^{14}$ g, kinetic energy $E_k = 1.9 \cdot 10^{29}$ erg. But the data of the second order Fit approximating the dependence of the CME height on time determined that the mass ejection velocity at altitudes of up to 20 R_s is equal to $V_{cme} \approx 400$ km/s. Here, R_s is the solar radius. The quality of the images of the stealth-CME in LASCO FOV is really poor that it is typical for images of many stealth-CMEs as many researchers note early. This stealth-CME was also detected by COR2 coronagraph included in the Sun-Earth Connection Coronal and Heliospheric Investigation (SECCHI; Howard et al. (2008)) package of instruments on board of the spacecraft Solar-Terrestrial Relations Observatory A, B (STEREO; Kaiser et al., 2008).

We analyzed the formation stage of this stealth-CME basing on high temporal resolution and high spatial resolution multiwave data provided by Atmospheric Imaging Assembly instruments (AIA, Lemen et al., 2012) on board Solar Dynamics Observatory (SDO; Pesnell et al., 2012). AIA presents simultaneous multiple high-resolution full-disk images of emission corona and transition region up to 0.5 Rs above the solar limb. AIA spatial resolution is about 0.6 arcsecs; the temporal resolution is 12 seconds cadence.

In present paper, presumably, for the first time, variations of the photospheric magnetic field in probable stealth-CME initiation source region are studied as well. To study the magnetic field variations in this region we used the photosphere magnetic field vector measurements from the Helioseismic and Magnetic Imager (HMI, Schou et al., 2012) and full-disk magnetograms obtained with 4096×4096 CCD matrix camera, pixel size is about 0.5 arcsec, the temporal resolution is 12 minute cadence (http://jsoc.stanford.edu/ajax/exportdata.html). We corrected HMI data using a more accurate and faster method proposed in paper Rudenko et al. (2014) to solved the π-ambiguity problem.

To find the probable location of the stealth-CME source region and to detect various manifestations of solar activity therein, we used the solar observations in several spectral AIA channels, i.e. on 93Å (temperature that corresponds to emission peak T = $6.5 \cdot 10^6$ K), 304 Å (T ≈ $0.05 \cdot 10^6$ K), 171 Å (T = $0.6 \cdot 10^6$ K), 193Å (T = $1.6 \cdot 10^6$ K), 211Å (T = $2 \cdot 10^6$ K), and 131Å (T = $10.1 \cdot 10^6$ K)) images. Temperature response functions for the AIA channels were listed by Boerner et al. (2012), Lemen et al. (2012), and in Fig. 4 in Downs et al. (2012).

The response of the geomagnetic field to the CME arrival was studied using data from (https://omniweb.gsfc.nasa.gov/), and from IMAGE magnetometer network (http://space.fmi.fi/image/). Dst-index is used as a measure of global geomagnetic disturbance; AL-index is used to evaluate the substorm intensity.

As mentioned above, we suggest a new approach to detect the source location and initiation time of a stealth-CME formation and the case study of the stealth-CME observed in LASCO C2 FOV on 2010 June 16.

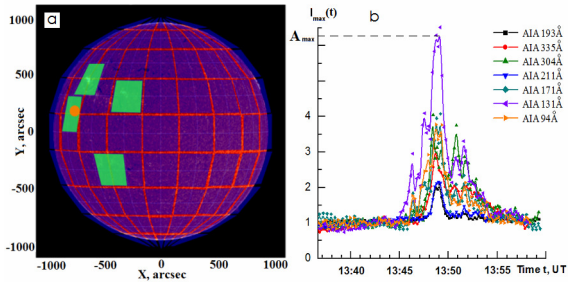

Fig. 2. a) – The visible part of the lower solar corona with green-colored segments, that show the regions of sharp increasing of the EUV emission (or EUV micro-flare) in different SDO/AIA channels before the stealth-CME occurred in the LASCO C2 FOV on 2010 June 16. Orange-colored circle points the area with the highest-intensity EUV micro-flare; b) - time dependence of the maximum emission intensity $I_{max}(t)$ in every of AIA channels in the area marked by orange.

It is based on our hypothesis that any forms of solar activity could be followed a stealth-CME initiation stage. For example, it could be a short-time small-scale solar activity as EUV emission bursts in different spectral ranges, occurring at several positions simultaneously or subsequently, or activation and eruption of magnetic loop structures.

First of all, we estimated the moment of probable appearance solar activity followed the stealth-CME formation in the emission corona. Using CME catalog data (https://cdaw.gsfc.nasa.gov/CME_list/) we calculated the average velocity of the stealth-CME moving from the solar surface to the

lower boundary (R = 2.83 R_s) of LASCO C2 FOV. It's equal about 55 km/s. Taking into account this velocity, we estimated time of the CME moving from R = R_s to R = 2.83 R_s, and concluded that the CME could begin to form later than 08:40 UT. We assumed that from this moment it is possible to appearance of any solar activity followed the stealth-CME formation.

For that it is necessary to split the visible part of the Sun into [200"×200"] segments as shown in Fig. 2a. We plotted time dependence of the maximum emission intensity $I_{max}(t)$ in every of AIA channels and within every segment. As a result, we found the low-intensity bursts of EUV emission within the four segments that are marked by green color in Fig. 2(a). Then, EUV emission intensity values I_a in the each selected AIA channel were normalized to the average emission intensity value of the quiet Sun I_q at any given time period between 08:44 UT and 14:50 UT.

To detect I_q we selected an area outside of the EUV emission burst location within every of four green-colored segments, then we calculated the average intensity value I_q within selected area. As a result, in every of the four segments we calculated the normalized micro-burst-intensity time dependence $I_n(t)=I_a(t)/I_q(t)$ and maximum of $I_n(t)$ in considered interval ($I_{max}(t)$). The highest-intensity A_{max} was found in one of the selected green-colored segments closed to the eastern solar limb. It allowed us to choose the segment with the small-time small-scale solar activity as the most likely the stealth-CME initiation source. This segment and the stealth-CME in LASCO C2 FOV were found in the same quarter (NE) that indirectly confirmed our assumption. The highlighted segment should be the source of a sharp short-time EUV intensity increase in different AIA channels (see orange-colored segment in Fig. 2a). Later, we studied small-scale solar activity only within the selected segment.

If we also find the location of the stealth-CME FS formation within the orange-colored segment it would be a good proof that our approach is correct. To find the stealth-CME FS we used data from all AIA channels but the well-known AIA 193 Å channel has proven to be more preferable for analyzing. We have computed the running difference images of the selected segment for the time interval from 8:40 UT to 14:50 UT on 2010 June 16.

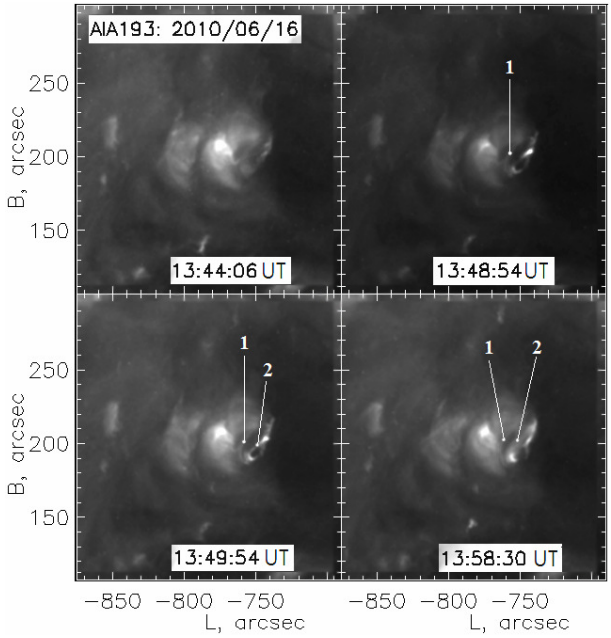

Fig. 3. Images of the solar disk part with the CME initiation source region, where the loop-like structures with the footpoint brightenings were observed, here 1 is the loop-like structure 1 observed in time interval from 13:48:54 UT to 13:53:06 UT, 2 is the loop-like structure 2 observed in time interval from 13:50:18 UT to 13:53:30 UT (velocity profiles of the loop-like structures you can see on Fig. 5).

3 - Results

3-1-Small-scale small-time low coronal signatures in Stealth CME initiation source

To study the morphology of CMEs formation and to find the small-scale small-time solar activity, we used methods listed above and data of several AIA channels. Figure 2b shows the ratios of the maximum emission intensity value I_a to the average quiet area intensity value I_q in the probable stealth-CME source region in different AIA channels, $I_n(t)=I_a(t)/I_q(t)$. More high-intensity emission was observed in AIA 131 Å, and the weakest one in was found in AIA 211 Å. We also note that EUV intensity was slowly increased in AIA 131 Å channel ten minutes before the sharp intensity increasing. In Fig 2b one can also see that duration of the EUV burst observed in AIA 131 is maximum and it is the shortest in AIA 211 Å channel. The EUV emission source regions located on the solar disk have small size (S_{SR} < [20"×20"]). Later we will call them "small-scale emission elements".

We must take into account that small-scale emission elements at different time moments correspond to different observation structure objects in the orange-colored region in Fig. 2. As it was noted above, during the considered interval from 13:45 UT to 13:52 UT the EUV micro-burst (or EUV micro-flare) was mainly observed in AIA 131 Å channel (see Fig. 2b). In the same time interval we found the footpoint brightenings at the base of a loop-like structures that are mainly visible in the AIA 193 Å channel (Fig. 3c, d). Simultaneously, the emission intensity sharply increases in one of the footpoint brightenings at the base of a loop-like structure in the AIA 193 Å (Fig. 3c).

Two loop-like structures were distinctly seen on solar running-difference images in AIA 193 Å channel at ≈ 13:45 UT (Fig. 3d). The loop-like structure with the footpoint brightenings became more long and wide at about 13:53 UT. The expansion and shifts of this loop-like structure were determined (Fig. 3a, b). Basing on 304 Å and Hα data observations no filaments were found in the orange-colored region. It looks like a hot magnetic flux rope but it could be a post-eruptive loop as well. We were able to find the shifts of the hot magnetic flux rope from its initial location and consequently its velocity for the short-time interval that was identified above (Fig. 5). This may be due to the start movement direction of this structure in studied time interval was close to line-of-sight motion direction. Thus, we observed the EUV micro-flare, activation and motion of small-scale loop-like structures, for the short period of time. Besides, sharp increased EUV brightness corresponds to the footpoint brightenings at the base of a loop-like structure.

3-2-Frontal structure of Stealth-CME

As far as we know no stealth-CME frontal structure in lower solar corona was registered yet. We present the case study when the identification of the stealth-CME frontal structure became possible.

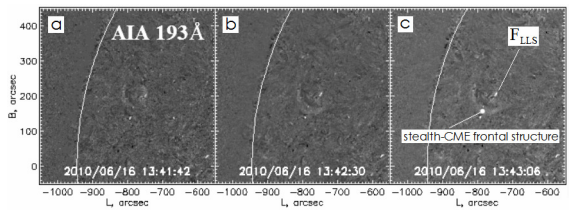

Fig. 4. Formation of the stealth-CME frontal structure on the solar disk images in AIA 193 Å channel in different moment of time. The fragment of the stealth-CME frontal structure is seen as curved band of increased brightness (here, F_{LLS} is the footpoint brightening at the base of a loop-like structure).

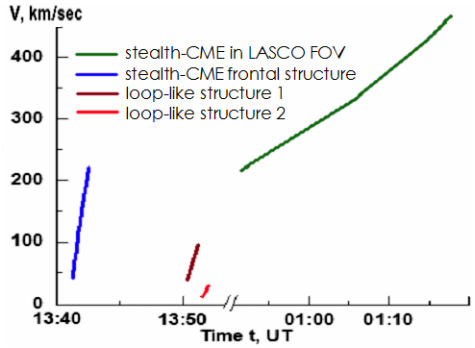

Fig. 5. Velocity profiles of the stealth-CME frontal structure in the FOV of SDO\AIA 193 Å imager, the loop-like structures (1 and 2) in the SDO\AIA 193 Å FOV and the stealth-CME in LASCO coronagraph FOVs.

Frontal structure of the stealth-CME on 2010 June 16 was more clearly observed on the running difference images in AIA 193 Å channel (Fig. 4). FS was detected as a part of the extended ring-like structure encircling the region of the EUV micro-flare (Fig. 2b) and loop-like structures (see Fig. 3.). The stealth-CME FS formation lasted for about 3 min. As we noted above, in most cases the FS formations are caused a filament eruption (or a magnetic flux-rope of another type) (Fainshtein and Egorov, 2015; Grechnev et al., 2016). We established that no filament eruption precedes the analyzed stealth CME therefore a trigger of the stealth-CME FS formation is unknown.

Let's note that EUV micro-flare started in a few minutes after the stealth-CME FS was already formed. It means that this EUV micro-flare is a result of the disturbance in the lower solar corona caused by the FS propagating.

So the stealth-CME FS, EUV micro-flare, and the activation of loop-like structures are detected in the same area on the solar disk we can conclude that our approach allows to locate the stealth-CME initiation source. Figure 5 shows the stealth-CME FS velocity profiles in the FOVs of SDO\AIA 193 Å imager and LASCO coronagraphs. From two time dependences of the CME velocity in SDO FOV and LASCO FOV in Fig. 5, one may assume, that the stealth-CME FS velocity reachs the maximum between 13:43 UT and 14:54 UT. The velocity profile of small-scale structures observed on AIA 193 Å images are demonstrated as well.

3-2- Some Quantitative Estimates

let's estimate a properties of EUV burst is followed the formation of the stealth-CME on 2010 June 16 in AIA 193 Å and 131 Å channels.

When $I_n(t)=l_a(t)/l_q(t)$ reaches the maximum in AIA 193 Å channel, the emission intensity maximum I_a is equal to 9653.6, the average emission intensity of quiet Sun I_q is equal to 4610.6, exposure time T_{exp} is equal to 2.90089 seconds. Hence, the ratio I_a/T_{exp} is equal to 3327.85 per second, and I_q/T_{exp} is equal to 1589.4 per second. At the same time the AIA 131 Å channel emission I_a is equal to 1052.8, I_q is equal to 161.5, T_{exp} is equal to 2.900849 seconds, I_a/T_{exp} is equal to 362.9 pixel-intensity per second, I_q/T_{exp} is equal to 55.7. It is interesting to compare these emission parameters of CME-related different X-ray flares, for example, to powerful flares and micro-flares. We estimated the these parameters, measured in the GOES M6.3 flare region with N15W03 coordinates on solar disk on March 9 at 03:22 UT. Note that the different exposition time is used for registeration of real emission intensity of X-ray flares in each pixel. To detect the solar images without underexposure and light-striking effects for observation of CME formation associated with powerful X-ray flare the optimum exposition time T_{exp} is equal 0.03916 seconds. And in this case, I_a/T_{exp} is equal 199402.4, I_q/T_{exp} is equal 160.8 in AIA 193 Å channel. Thus, according to rough estimates, the difference between the I_n of micro-burst and powerful flare is almost three orders of magnitude that is by no means negligible!

We also compared the kinetic energy of the CME frontal structure and the kinetic energy of each small-scale structures within the mass ejection source region observed in AIA 193 Å channel. For our assessment of the kinetic energies of the longest loop-like structure and FS of the stealth-CME (see Fig. 3d and Fig. 4) we used formula: $E_{k\_fr} / E_{k\_fs} = N_{fr}V_{fr}(S_{fr})^2 / (N_{fs}V_{fs}(S_{fs})^2)$.

Here, E_{k_fr} is the kinetic energy of the small-scale structure, E_{k_fs} is the kinetic energy of FS, N_{fr} and N_{fs} are the proton density of the above structures, V_{fr} and V_{fs} are space sizes of the structures, S_{fr} and S_{fs} are their speeds respectively. V_{fr} and V_{fs} were calculated as a cylinder volume multiplied by 1.5 (it's a rough estimate of the contribution of the footpoint at the base of a loop-like structures) and a volume of spherical layer or loop structure respectively. N_{fr}/N_{fs} was assumed to be equal to the ratio of emission intensities of the above structures in AIA 193 Å channel. It's also a rough estimation of N_{fr} and N_{fs} values. If the FS is a spherical layer then $V_{fr}/V_{fs} = 1.1 \cdot 10^{-2}$, but if it has a loop-like form then $V_{fr}/V_{fs} = 9.3 \cdot 10^{-2}$. According to our estimates, S_{fr}/S_{fs} is equal 0.0123. Then for FS of spherical layer, the ratio of the flux-rope kinetic energy to the CME FS one is $E_{k\_fr}/E_{k\_fs} = 4.06 \cdot 10^{-4}$. And for FS of loop-like structure, it's ~ $3.73 \cdot 10^{-3}$. For moving structures of another forms, the ratio of kinetic energies is even less. Thus, the energy of the loop-like structure motion observed after the onset of the stealth-CME FS formation is just a small share of the FS kinetic energy.

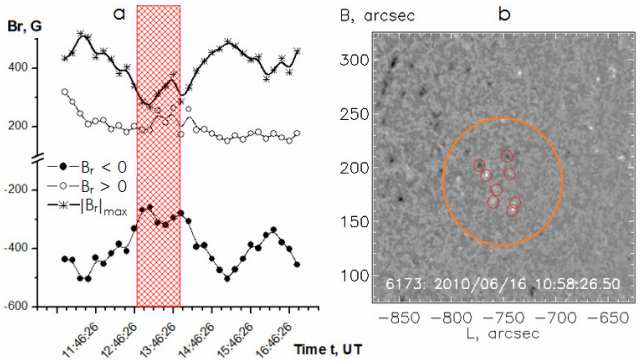

Fig. 6. Time dependences of the magnetic field maximum radial component Br of different polarity (Br < 0 and Br > 0) and the module of the magnetic field maximum radial component $|Br|_{max}$ in the stealth-CME initiation source area.

3 – 4 Magnetic field variations associated with stealth CME formation

As far as we know, the magnetic field variations associated with stealth-CME formation have not been investigated before now. We studied the magnetic field variations within the area of the stealth-CME initiation source as well.

Fig. 6a shows the time dependences of the magnetic field maximum radial component Br of different polarity ($B_r < 0$ and $B_r > 0$) and the module of the magnetic field maximum radial component $|B_r|_{max}$ in the stealth-CME initiation source area (it's about ~100"×100" square). The vertical strip marks a very short time interval from 13:02 UT to 14:04 UT with B_r unusual behavior, i.e. Br stopped decreasing, then sharply increased and dropped again. Later 14:04 UT $|B_r|_{max}$ and Br of negative polarity ($Br < 0$) increased, but B_r of positive polarity ($B_r > 0$) decreased and did not change significantly.

Note this short-time interval includes the FS formation period and the period of EUV micro-flare observation in different AIA channels. Thus, the stealth-CME formation in the supposed source area is preceded by noticeable variations of the magnetic field. From Fig. 2b and Fig. 6a one can see that the onset EUV micro-flare in AIA 131 Å coincided with maximum of Br in considerable interval.

Presumably, increasing of Br in the interval between 13:02 UT and 14:04 UT is caused by the emergence of a new magnetic flux.

|Br|max decreased close to 14:04 UT that could be caused by the magnetic field configuration changes associated with new magnetic flux in the stealth-CME initiation source area.

We overlapped the π-ambiguity resolved vector magnetograms (Fig. 6b) on images in AIA 131 Å channel (Fig. 6b), found the region with EUV micro-flare in the magnetograms and identified a micro-scale area where Br increased, so-called "magnetic nodes". The "magnetic nodes" are neither sunspots nor pores. We have a plan to continue studding of "magnetic nodes".

3 – 5- Geomagnetic activity as response to Stealth CME approach

Taking into account the considered CME velocity, it was supposed that the stealth-CME on 2010 June 16 could reach the Earth's orbit on 21-22 June. Fig. 7 shows the Interplanetary Magnetic Field (IMF) components (|B| and Bz component), parameters of the Solar Wind (SW) such as speed, the proton density, the proton temperature of the solar wind, and the indices of geomagnetic activity AL and Sym/H (analog of Dst) on 21-22 June 2010.

Analysis of the interplanetary magnetic field (IMF) and the solar wind parameters showed that the interplanetary shock (SI) reached the magnetosphere at ~ 02:00 - 03:00 UT on 21 June 2010, when the weak jumps of the solar wind proton density (~2 $cm^{-}3$) and velocity (from 380 up to 420 km/s), and changing of the IMF Bz from negative to positive value were fixed. Magnetic Cloud (MC) reached the Earth at about 05:00 UT (http://www.srl.caltech.edu/ACE/ASC/DATA/level3/icmetable2.htm). Here, one can observe the jump of the SW proton density (from 5 up to 9 cm^{-3}) and the SW proton temperature drops with increasing IMF |B| and low-speed SW. Note that, increased AL index is observed in the vicinity of both front and back boundary of interplanetary CME (ICME). In this case, according to the catalog, ICME in question has the signs of MC. We can note that after SI occurred, the IMF Bz varied slightly near zero. There were no conditions for development of magnetic storm; Dst index remained very small. But during the short period (05:00 - 06:00 UT), when the IMF Bz was negative, we observed development of the weak auroral activity reflected in AL index. The substorm (till -250 nT) was registered in the night side of the magnetosphere at Fort Churchill station (it is not seen here). But no increase in geomagnetic activity was observed after 09:00 UT due to the fact that the IMF Bz became positive and did not change its sign during long time. The IMF Bz changed to negative values at ~14:00 UT on 22 Jun and caused new surge of weak auroral geomagnetic activity (AL ~ - 200 nT), which could be a characteristic of the MC back boundary.

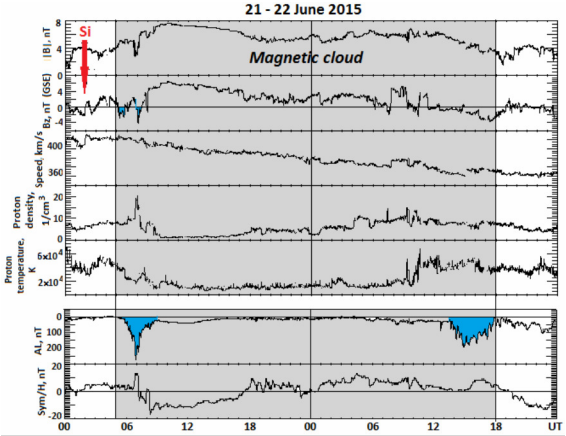

Fig. 7. Variations of |B| and Bz components of the interplanetary magnetic field, the velocity, solar wind proton density and temperature, the geomagnetic indices of the substorm activity AL and the magnetic storm intensity Sym/H (Dst) on 2010 Jun 21-22 (red arrow indicates the moment of SI approach; magnetic cloud area is colored by gray).

4 - CONCLUSIONS

We presented of a new approach to detect source location and initiation time of a stealth-CME on the solar disk and case study of the stealth-CME observed in LASCO C2 FOV on 2010 June 16 at 14:54:05 UT. Details of the stealth-CME formation were also studied. The response of the magnetosphere and the magnetic field of the Earth to this stealth-CME is discussed as well.

Our results may be formulated as follows:

Formation stage of the stealth-CME observed by LASCO coronagraphs on 2010 June 16 was associated with various manifestations of short-time small-scale solar activity, such as the sharp increasing of the EUV emission intensity in the different SDO/AIA channels, the activation and moving of the small-scale loop-like structures (or the magnetic flux ropes).

The proposed new approach have made it possible, to detect, for the first time, the formation of stealth CME frontal structure on running-difference images in AIA 193 Å channel.

Velocity profile of the stealth CME frontal structure is determined. It's shown that the profile neither gradual nor pulse.

For the first time, magnetic field variations in the stealth-CME initiation source region were studied. The behavior of the magnetic field maximum radial component Br of positive and negative polarity and the module of the magnetic field maximum radial component $|Br|_{max}$ was revealed in the mass ejection source region during the stealth-CME frontal structure formation. The Br decreased before and increased after the eruptive event.

The stealth-CME arrival at the Earth did not lead to a noticeable geomagnetic field disturbance described by the Dst-index. The passage of the stealth-CME front close to the Earth was followed by a weak substorm. It has been also concluded that the stealth-CME structure on the Earth's orbit is similar to a magnetic cloud structure.

Acknowledgment

The authors thank the SOHO/LASCO, SDO/AIA, SDO/HMI, GOES teams for a possibility to freely use the data from those instruments. The study was done with budgetary funding of Basic Research program II.16.

References

Alzate, N., and Morgan, H.: 2017, Astrophys.l J. 840, 103, 1–14.

Boerner, P., Edwards, C., Lemen, J., Rausch, A., Schrijver, C., Shine, R., Shing, L., Stern, R., Tarbell, T., Title, A., et al.: 2012, Solar Phys. 275, 41.

D'Huys, E., Seation, D.B., Poedts, S., and Berghmans, D.: 2014, Astrophys. J. 795, 1-12.

Downs, C., Roussev, I.I., van der Holst, B., Lugaz, N., Sokolov, I.V.: 2012, Astrophys. J. 750, 134.

Feynman, J. and Martin S. F.: 1995. J. Geophys. Res. 100, 3355.

Fainshtein, V. G. and Egorov, Ya. I.: 2015, Advances. Space Res. 55, 798.

Gallagher P. T., G. R. Lawrence, and B. R. Dennis: 2003, Astrophys. J., 588, L53.

Grechnev V.V., Uralov A.M,. Kochanov A.A., Kuzmenko I.V., Prosovetsky D.V., Egorov Y.I., Fainshtein V.G., Kashapova L.K.: 2016, Solar Phys. 291, 1173.

He W.Y., Liu, D., Hu, H., Wang, R. and Zhao, X. A.: 2018, The Astrophysical Journal, 860:78 (7pp).

B. Heber, D. Galsdorf, J. Gieseler, K. Herbst, C. Wallmann, M.Dumbović, B. Vršnak A. Veronig. M. Temmer, and C. Moestl. THE XIII-TH HVAR ASTROPHYSICAL COLLOQUIUM "PHYSICS OF THE SOLAR ATMOSPHERE", 22 - 26 SEPTEMBER 2014, HVAR, CROATIA.

Heber B., Wallmann, C., Galsdorf, D., Herbst, K., Kühl, K., Dumbovic, M., Vršnak, B., Veronig, A., Temmer, M., Möstl, M, Davilla, S.: 2015, Cent. Eur. Astrophys. Bull., 39, no. 1, 75.

Howard, R.A., Moses, J.D., Vourlidas, A., Newmark, J.S., Socker, D.G., Plunkett, S.P., Korendyke, C.M., Cook, J.W., Hurley, A., Davila, J.M., et al.: 2008, Space Sci. Rev. 136, 67.

Howard, T.A., and Harrison, R.A.: 2013, Solar Physics, 285, 269.

Kaiser, M.L., Kucera, T.A., Davila, J.M., St. Cyr, O.C., Guhathakurta, M. and Christian, E.: 2008, Space Sci. Rev. 136, 5.

Kilpua, E. K. J., Mierla, M., Zhukov, A. N., et al.: 2014, Solar Phys, 289, 3773.

Lemen, J.R., Title, A.M., and Akin, D.J. et al.: 2012, Solar Phys. 275, 17.

Ma, S., Attrill, G. D. R., Golub, L., and Lin, J.: 2010, Astrophys. J. 722, 289. doi:10.1088/0004-637X/722/1/289

Nitta, N., and Mulligan, T.: 2017, Solar Phys. 292, 125. DOI 10.1007/s11207-017-1147-7.

Pesnell, W.D., Thompson, B.J., and Chamberlin, P.C.: 2012, Sol. Phys., 275, 3.

Robbrecht, E., Patsourakos, S., and Vourlidas, A.: 2009, Astrophys. J. 701, 283.

Rudenko, G.V., and Anfinogentov, S. A.: 2014, Solar Phys. 289. 1499.

Schou, J., Scherrer, P. H., Bush, R. I., Wachter, R., Couvidat, S., Rabello-Soares, M., Bogart, R. S., Hoeksema, J. T., Liu, Y., Duvall, T. L., and 11 coauthors.: 2012, Solar Physics, 275, 229.

Schmieder, B., De´moulin, P., Aulanier, G.: 2013, Advances Space Res., 51, 1967.

Sterling, A. C., Chifor, C., Mason, H. E., Moore, R. L., and Young, P. R.: 2010, Astron. Astrophys. 521, A49.

Zagainova, Iu. S., and Fainshtein, V. G. 2015. Advances Space Res. 55, 822.